Molecular Cancer Therapeutics

The MDM2 Inhibitor AMG 232 Demonstrates Robust Antitumor Efficacy and Potentiates the Activity of p53-Inducing Cytotoxic Agents

Jude Canon[1], Tao Osgood[1], Steven H. Olson[2], Anne Y. Saiki[1], Rebecca Robertson[1], Dongyin Yu[1], John Eksterowicz[3], Qiuping Ye[4], Lixia Jin[4], Ada Chen[3], Jing Zhou[3], David Cordover[5], Stephen Kaufman[5], Richard Kendall[1], Jonathan D. Oliner[1], Angela Coxon[1], and Robert Radinsky[1]

Abstract

p53 is a critical tumor suppressor and is the most frequently inactivated gene in human cancer. Inhibition of the interaction of p53 with its negative regulator MDM2 represents a promising clinical strategy to treat p53 wild-type tumors. AMG 232 is a potential best-in-class inhibitor of the MDM2–p53 interaction and is currently in clinical trials. We characterized the activity of AMG 232 and its effect on p53 signaling in several preclinical tumor models. AMG 232 binds the MDM2 protein with picomolar affinity and robustly induces p53 activity, leading to cell-cycle arrest and inhibition of tumor cell proliferation. AMG 232 treatment inhibited the *in vivo* growth of several tumor xenografts and led to complete and durable regression of MDM2-amplified SJSA-1 tumors via growth arrest and induction of apoptosis. Therapeutic combination studies of AMG 232 with chemotherapies that induce DNA damage and p53 activity resulted in significantly superior antitumor efficacy and regression, and markedly increased activation of p53 signaling in tumors. These preclinical data support the further evaluation of AMG 232 in clinical trials as both a monotherapy and in combination with standard-of-care cytotoxics. *Mol Cancer Ther; 14(3); 649–58. ©2015 AACR.*

Introduction

The p53 tumor suppressor regulates critical cellular processes such as cell-cycle control and response to cellular stresses such as hypoxia, DNA damage, or oncogene activation (1, 2). Upon activation, p53 controls a complex signaling network that regulates cell-cycle progression, DNA repair, senescence, and apoptosis. These downstream responses protect cells from replicating harmful genetic lesions that can lead to deregulated growth and tumor development. Because of its critical function, inactivation of p53 in tumor cells provides a growth advantage and is often considered a necessary step in tumor formation (1). Approximately 50% of human tumors harbor a mutated *TP53* gene (3). In the remaining tumors, *TP53* is wild-type but its full activation and function may be blocked by other mechanisms such as its negative regulator MDM2, which keeps p53 levels low in nonstressed cells. MDM2 controls p53 activity by several mechanisms, including blocking its transactivation domain, acting as an E3 ubiquitin ligase to target p53 for degradation, and transporting p53 out of the nucleus (1, 4–6). Inhibition of the MDM2-p53 protein–protein interaction would block each of these mechanisms and is, therefore, an attractive target for restoration of p53 activity in tumor cells. Preclinical studies have indeed demonstrated restoration of p53 activity and inhibition of tumor growth by small-molecule MDM2 inhibitors (7–11). Previously, we reported the *de novo* design of AM-8553 as a potent and selective piperidinone inhibitor of the MDM2–p53 interaction (10). Further research led to the discovery of AMG 232, which has excellent *in vivo* properties and is the most potent MDM2 inhibitor described to date (12). Here, we present the pharmacologic characterization of AMG 232, a compound that exhibits robust antitumor activity *in vivo* and potentiates the antitumor effects of DNA-damaging, p53-inducing chemotherapeutics.

[1]Department of Oncology Research, Amgen Inc., Thousand Oaks, California. [2]Department of Medicinal Chemistry, Amgen Inc., San Francisco, California. [3]Department of Molecular Structure, Amgen Inc., San Francisco, California. [4]Department of Pharmacokinetics and Drug Metabolism, Amgen Inc., San Francisco, California. [5]Department of Pathology, Amgen Inc., Thousand Oaks, California.

Note: Supplementary data for this article are available at Molecular Cancer Therapeutics Online (http://mct.aacrjournals.org/).

Corresponding Author: Jude Canon, Amgen, Inc., 1 Amgen Center Drive, Thousand Oaks, CA 91320. Phone: 805-447-3762; Fax: 805-375-8524; E-mail: jcanon@amgen.com

doi: 10.1158/1535-7163.MCT-14-0710

Materials and Methods

Cells

SJSA-1, HCT116, ACHN, NCI-H460, MOLM-13, RKO, MCF7, 22RV1, HT-29, PC-3, NCI-H82, NCI-SNU1, and MG-63 cells were purchased from the ATCC, and have since been authenticated by short tandem repeat analysis (PowerPlex 18D Kit from Promega). NCI-H2452, SW982, C32, SK-HEP-1, A375, RT4, RPMI-2650, MDA-MB-134-VI, NCI-H2347, and A427 cells were purchased from ATCC and used within 6 months. IGR-1 and CML-T1 cells were purchased from German Collection of Microorganisms and Cell Cultures (DSMZ) and used within 6 months. A375sq2 cells were generated by *in vivo* passaging A375 cells in mice (13).

HCT116 p53$^{-/-}$ cells were obtained from Bert Vogelstein. KS-1 and SNG-M were purchased from the Japanese Collection of Research Bioresources (HSRRB) and used within 6 months. G-401, G-361, LS174T cells (purchased from ATCC), EOL-1 cells (purchased from DSMZ) and KP-4 cells (purchased from HSRRB) were used after 6 months of purchase.

Surface plasmon resonance spectroscopy binding assay (Biacore)

As previously described in ref. (10).

Cell proliferation assays

Bromodeoxyuridine (BrdUrd) for HCT116 and ACHN cell assays, and EdU for SJSA-1 cell assay. As previously described in ref. (10).

p21 IC_{50} cell assay

As previously described in ref. (10).

Immunoblot analysis

Tumor cells were treated with DMSO (0.1%) or AMG 232 (0.1, 1, or 10 μmol/L). After 24 hours, protein lysates were collected, electrophoresed, and transferred to polyvinylidene difluoride membranes (Life Technologies). Primary antibodies: p53 (DO-1; Calbiochem), MDM2 (BD Pharmingen), p21 (R&D Systems), PUMA (Abcam), or β-actin–HRP (Sigma).

Cell viability assay (72 hours)

Cell lines were plated in 96- or 384-well plates at optimum initial seeding densities to ensure that cells did not reach confluency by the end of the assay. The cells were treated with DMSO control or AMG 232 at various concentrations for 72 hours. CellTiter-Glo Luminescent Cell Viability (Promega) or ATPlite 1step Luminescent (PerkinElmer) assay kits were used to determine the numbers of viable cells. Luminescence was measured with an EnVision Multilabel Reader (PerkinElmer) for each cell line at time zero (V_0) before the addition of compounds, as well as after 72 hours of compound treatment. Growth inhibition (GI) was calculated on a 200-point scale according to the following equations, where V_{72} was luminescence of DMSO control at 72 hours and T_{72} was luminescence of the compound-treated sample: if $T_{72} > V_0$, then $GI = 100 \times (1 - ((T_{72} - V_0)/(V_{72} - V_0)))$; if $T_{72} < V_0$, then $GI = 100 \times (1 - ((T_{72} - V_0)/V_0))$. GI values of 0, 100, and 200 represented uninhibited cell growth (i.e., DMSO control), cell stasis, and complete cell killing, respectively. Dose–response curves were generated using XLFit software (IDBS) to calculate IC_{50} values for AMG 232 in each cell line tested.

Animal studies

All animal experimental procedures were conducted in accordance with the guidelines of the Amgen Animal Care and Use Committee and the Association for Assessment and Accreditation of Laboratory Animal Care standards. All studies utilized 4- to 6-week-old female athymic nude mice (Harlan Laboratories, Hsd: Athymic Nude-*Foxn1*^{nu}). The mice were housed five per filter-capped cage in sterile housing in an environmentally controlled room (temperature 23 ± 2°C, relative humidity 50 ± 20%) on a 12-hour light/dark cycle. The mice were fed commercial rodent chow (Harlan Laboratories, #2920X) and received filter-purified tap water ad libitum. The mice were individually identified by microchips (Bio Medic Data Systems) that were implanted subcutaneously at least 2 days before the study.

Pharmacodynamic assays

Tumor cells (SJSA-1: 5×10^6 cells, HCT 116: 2×10^6 cells) were injected subcutaneously into the flank of female athymic nude mice in a 2:1 ratio of cells to Matrigel (BD Bioscience). AMG 232 was administered by oral gavage when average tumor size reached approximately 300 to 450 mm^3 (n = 4/group). Tumors were harvested after 1, 2, 4, 8, and 24 hours after dose (SJSA-1) or 6 hours after dose (HCT116) and snap-frozen in liquid nitrogen. Total RNA was purified using Qiagen RNeasy 96 kit (Qiagen). The levels of p21 and the housekeeping gene GAPDH were assayed from total RNA from each sample in technical duplicates by qRT-PCR. The qRT-PCR reactions were assayed on the Applied Biosystems Prism 7900HT instrument and the data were analyzed with Applied Biosystems SDS2.2 software. The SDS2.2 software calculated the p21 and GAPDH copy number in each of the tumor samples. The copy number of p21 was normalized to the copy number of the GAPDH, and the fold increase of normalized p21 levels were calculated relative to vehicle control for each sample. For MIC-1, plasma was collected at the time of sacrifice and MIC-1 was detected using R&D Quantikine Human MIC-1 Immunoassay (cat no. DGD150) following the manufacturer's instructions. The ELISA assay was read using a Spectramax M5 microplate reader using Softmax pro v4 (Molecular Devices).

Xenograft studies

SJSA-1 cells (5×10^6 cells with Matrigel at a ratio of 2:1), NCI-H460 cells (5×10^6 cells with Matrigel at a ratio of 2:1), A375sq2 (5×10^6 cells with Matrigel at a ratio of 2:1), or HCT116 (2×10^6 cells) were injected subcutaneously in the flank of female athymic nude mice (n = 10/group). Treatment began when tumors were established and approximately 200 mm^3. AMG 232 was administered once per day by oral gavage. Cisplatin, carboplatin, doxorubicin, and CPT-11 were dosed once per week by i.p or i.v. (doxorubicin) injection. Combination treatment studies were performed in a blinded manner. Tumor dimensions were assessed twice weekly with a Pro-Max electronic digital caliper (Sylvac) and tumor volume was calculated using the formula: length × width × height and expressed as mm^3. Data are expressed as mean ± SEM. Body weight was recorded twice weekly to assess tolerability (data not shown). Analysis of p21 mRNA at the end of the xenograft studies was performed as described for the p21 pharmacodynamic assay.

Detection of BrdUrd and cleaved caspase-3 in xenografts

Tumors were harvested 6 hours after the last treatment, formalin fixed, and processed into paraffin. Two hours before harvest, mice were intraperitoneally injected with BrdUrd (50 mg/kg). Tumor sections were immunostained for either BrdUrd or cleaved capsase-3 using commercial antibodies and counterstained with hematoxylin. Sections were scanned at ×20 via the Aperio Digital Scanner and positive nuclear densities were determined using Visiomorph image analysis software.

Statistical analysis

For *in vivo* AMG 232 dose–response efficacy studies, repeated-measures ANOVA (RMANOVA) followed by the Dunnett *post hoc* test for multiple comparisons was used to evaluate statistical

Table 1. Comparison of biochemical potencies of MDM2 inhibitors

Compound name	Biacore K_D (nmol/L)	Potency shift from AMG 232
RG7112	2.9	−64.4
SAR299155	2.7	−60
RG7388	0.15	−3.3
AMG 232	0.045	—

NOTE: Data represent mean ± SEM.

Table 3. Comparison of cellular potencies of MDM2 inhibitors in an SJSA-1 proliferation assay

Compound name	SJSA-1 proliferation IC_{50} (nmol/L)[a]	Potency shift from AMG 232
CGM097	931 ($n = 1$)	−102.3
RG7112	590.2 ± 21.0 ($n = 13$)	−64.9
SAR299155	214.2 ± 24.6 ($n = 4$)	−23.5
RG7388	45.4 ± 5.9 ($n = 2$)	−5.0
AMG 232	9.1 ± 2.9 ($n = 69$)	—

NOTE: Data represent mean ± SEM.
[a]Assays were conducted in the presence of 10% human serum.

significance of observed differences. For the combination studies, RMANOVA followed by the Dunnett *post hoc* test was used to compare the combination treatments with single-agent treatments. The *in vivo* pharmacodynamic and mechanism of action experiments were analyzed with ANOVA (Kruskal–Wallis) followed by the Dunnett *post hoc* test. All statistical analyses were performed using JMP software v8 interfaced with SAS v9.1 (SAS Institute, Inc.).

Results

AMG 232 potently inhibits the MDM2–p53 interaction

AMG 232 was discovered via optimization of AM-8553, our previously described piperidinone inhibitor of MDM2 (10). Further investigation into the *N*-alkyl substituent of this series led to the discovery of AMG 232 (Supplementary Fig. S1A), which exhibits significantly improved biochemical and cell-based potency, and *in vivo* properties (12). Based upon X-ray cocrystal structures of related molecules (12), a model of AMG 232 bound to MDM2 was developed. The model shows that the *m*-chlorophenyl, the *p*-chlorophenyl, and C-linked isopropyl fragments of AMG 232 bind to the Leu $26_{(p53)}$, Trp $23_{(p53)}$, and Phe $19_{(p53)}$ pockets of MDM2, respectively (Supplementary Fig. S1B). The carboxylic acid forms a salt bridge with His 96 and the isopropyl sulfone forms a novel interaction with the glycine shelf region of MDM2. As previously reported (12), AMG 232 inhibited the p53–MDM2 interaction in a cell-free homogeneous time resolved fluorescence (HTRF)-binding assay with an IC_{50} of 0.6±0.4 nmol/L. Consistent with those data, Biacore assays revealed that AMG 232 binds to MDM2 with a K_D of 0.045 nmol/L. To understand the relative biochemical potencies of AMG 232 compared with other recently described MDM2 inhibitors, a head-to-head Biacore assay was conducted with RG7112, SAR299155, and RG7388 (9, 11, 14). AMG 232 was the most potent inhibitor in this assay (Table 1).

AMG 232 induces p53 signaling and inhibits tumor cell proliferation

Activation of p53 signaling was determined by measuring induction of p21 mRNA, a direct transcriptional target of p53, in three p53 wild-type tumor cell lines (SJSA-1, HCT116, and ACHN). AMG 232 treatment caused robust p21 mRNA induction between 9.76- and 34.9-fold with IC_{50} values ranging from 12.8 to 46.8 nmol/L (Table 2). Similarly, cell proliferation assays demonstrated that AMG 232 treatment potently inhibited proliferation of these tumor cell lines with IC_{50} values ranging from 9.4 to 23.8 nmol/L (Table 2). To compare relative cellular potencies with other MDM2 inhibitors, also including recently described CGM097 (15), we ran head-to-head cell proliferation assays in the MDM2-amplified SJSA-1 cell line in the presence of 10% human serum. AMG 232 was the most potent compound in this assay (Table 3). We then assayed a broader panel of tumor cell lines, including both p53 wild-type ($n = 23$) and mutant ($n = 7$) lines representing a range of tumor types and genetic backgrounds, and determined the effect of AMG 232 treatment on cell growth over a 72-hour period. In the 23 p53 wild-type cell lines we evaluated, AMG 232 treatment inhibited the growth of cells with IC_{50} values ranging from 0.1 to 1 μmol/L (Fig. 1A and C). As expected, there was no significant effect on growth of the p53-mutant lines. To understand the maximum effect of AMG 232 treatment on tumor cells, the degree of antiproliferative activity was plotted on a 200-point scale where 200% represented complete cell killing, and 100% represented cytostasis (complete inhibition of growth) compared with DMSO-treated controls. Antitumor activities ranged from 45% to 200% in the p53 wild-type cell lines, whereas the p53-mutant lines showed little to no effect (Fig. 1B and C).

For further evaluation of p53 pathway activity, we assessed protein levels of p53 itself and p53 targets p21, MDM2 (which forms a feedback loop with p53) and PUMA (a marker of p53 apoptotic activity) in three cell lines. AMG 232 treatment caused a dose-dependent accumulation of p53 and increased p21, MDM2, and PUMA proteins in both MDM2-amplified SJSA-1 cells and non–MDM2-amplified HCT116 cells (Fig. 2A). There was no effect on p53, MDM2, p21, or PUMA protein levels in p53-mutant HT-29 cells indicating the p53-dependent effects of AMG 232. We measured p53, MDM2, and p21 proteins in an additional four tumor cell lines treated with AMG 232. Again, AMG 232 treatment caused stabilization of p53 protein, and induction of MDM2 and p21 proteins in p53 wild-type cells (Supplementary Fig. S2).

AMG 232 activates p53 pathway activity *in vivo*

To determine the effect of AMG 232 treatment on the p53 pathway *in vivo*, p21, MDM2, and PUMA mRNA transcript levels were measured as pharmacodynamic readouts in

Table 2. Cellular activity of AMG 232 in tumor cell lines

Cell line	p21 IC_{50} (nmol/L)[a]	p21 max. fold induction	Proliferation IC_{50} (nmol/L)[a]
SJSA-1	46.8 ± 14.5 ($n = 10$)	34.90 ± 4.09 ($n = 10$)	9.4 ± 2.9 ($n = 69$)
HCT116	20.8 ± 9.7 ($n = 8$)	9.76 ± 2.10 ($n = 8$)	11.3 ± 6.0 ($n = 9$)
ACHN	12.8 ± 6.0 ($n = 4$)	11.45 ± 1.36 ($n = 4$)	23.8 ± 5.3 ($n = 4$)

NOTE: Data represent mean ± SEM. n = number of assays conducted.
[a]Assays were conducted in the presence of 10% human serum.

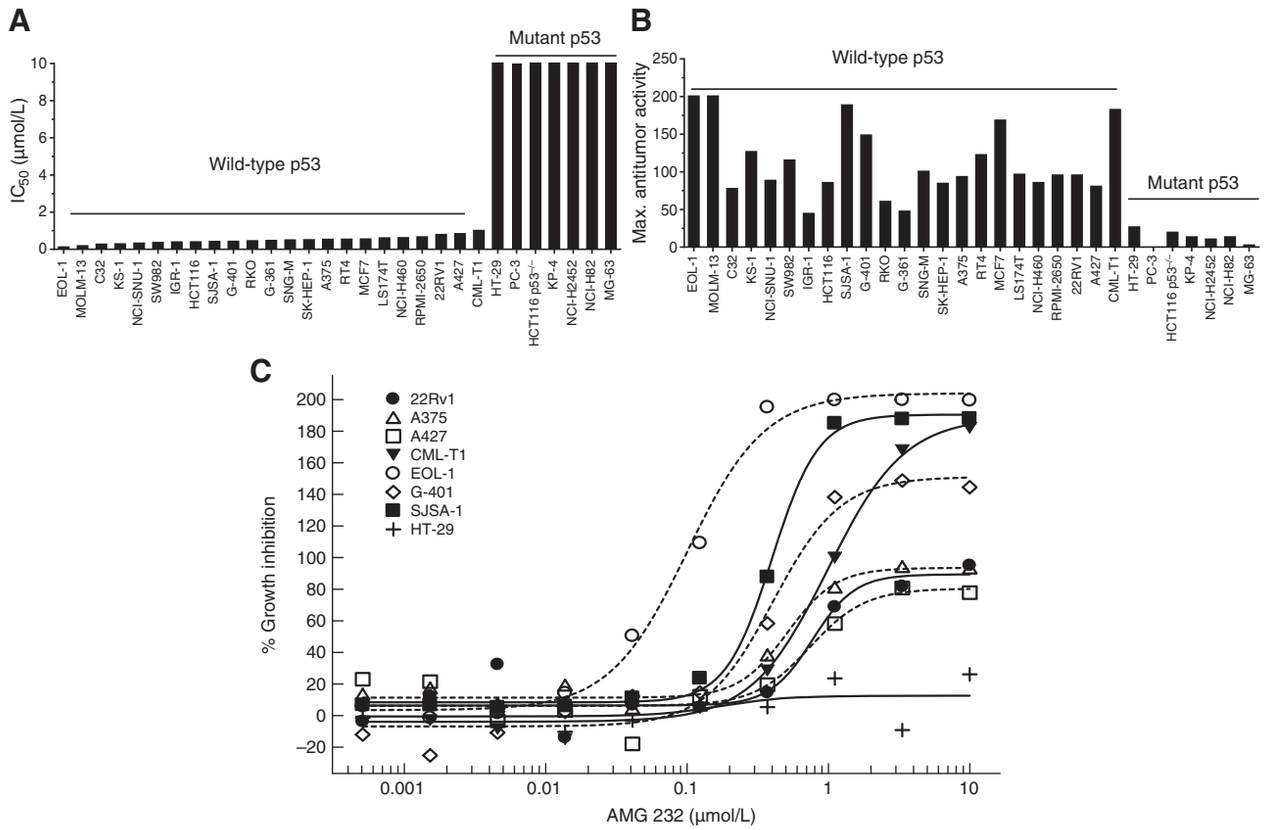

Figure 1.
AMG 232 inhibits cell proliferation in p53 WT cell lines *in vitro*. A, cell growth IC_{50} plot of 30 tumor cell lines treated with AMG 232 for 72 hours. B, maximum antitumor activity of AMG 232 treatment (10 μmol/L). 200% = complete cell killing, 100%, stasis; 0%, uninhibited cell growth (DMSO control). C, representative AMG 232 dose–response curves for a subset of the cell lines in A and B. Tumor cells were treated with DMSO control or AMG 232 (0.0005–10 μmol/L, 3-fold serial dilutions) for 72 hours. All cell lines shown in C are wild-type for p53, except HT-29, which is p53 mutant.

SJSA-1 and HCT116 tumors. Tumors treated with vehicle served as a negative control and indicated the baseline mRNA levels. AMG 232 treatment resulted in time- and dose-dependent induction of p21 mRNA in SJSA-1 tumors (Fig. 2B, top). p21 levels peaked at 4 hours after dose, and achieved maximal induction of approximately 30-fold over control in the 75 mg/kg group. In the 10 and 25 mg/kg groups, p21 levels were significantly elevated from 1 to 8 hours after dose, and returned to baseline levels by 24 hours. However, in the 75 mg/kg group, p21 levels remained significantly elevated out to 24 hours after dose. Similar effects were observed on MDM2 and PUMA expression in SJSA-1 tumors, where AMG 232 treatment caused a >10-fold induction of these p53 targets after 4 hours (75 mg/kg group; Fig. 2B, bottom), and sustained elevation out to 24 hours after dose. AMG 232 treatment also caused a dose-dependent induction of p21, MDM2, and PUMA mRNA in HCT116 tumors (Fig. 2C). At 6 hours after dose, AMG 232 treatment of HCT116 tumor-bearing mice caused induction of p21 and MDM2 transcript levels by approximately 13-fold and approximately 4-fold over control (100 and 15 mg/kg, respectively). PUMA expression was also significantly elevated in HCT116 tumors, but the magnitude of PUMA induction (4-fold in 100 mg/kg group) was less than the other p53 targets, and less than PUMA induction observed in SJSA-1 tumors. For an additional pharmacodynamic readout of p53 pathway activity, we measured the secreted protein MIC-1 (human specific) in the plasma of AMG 232-treated, HCT116 tumor-bearing mice. MIC-1 protein was elevated by 6-fold (100 mg/kg) and 3-fold (15 mg/kg) after 6 hours of AMG 232 treatment (Fig. 2D). Taken together, the induction of p21, MDM2, PUMA, and MIC-1 indicated on-mechanism activation of the p53 pathway by AMG 232 treatment.

AMG 232 potently inhibits growth of tumor xenografts in mice

We evaluated the antitumor activity of AMG 232 in xenograft models representing different genetic backgrounds and various tumor types. All tumor cell lines utilized in xenograft models harbored wild-type p53. Daily oral administration of AMG 232 resulted in significant tumor growth inhibition (TGI) across all models (Fig. 3A, C, E, and G). SJSA-1, an MDM2 amplified osteosarcoma model, was the most sensitive to AMG 232 treatment with an ED_{50} of 9.1 mg/kg. In the highest dose group of 75 mg/kg, 10 of 10 tumors completely regressed and were undetectable after 10 days of treatment. AMG 232 treatment was stopped in this group after day 25, and mice were observed for an additional 50 days. There was no detectable SJSA-1 tumor regrowth in any of the mice. Additional xenograft

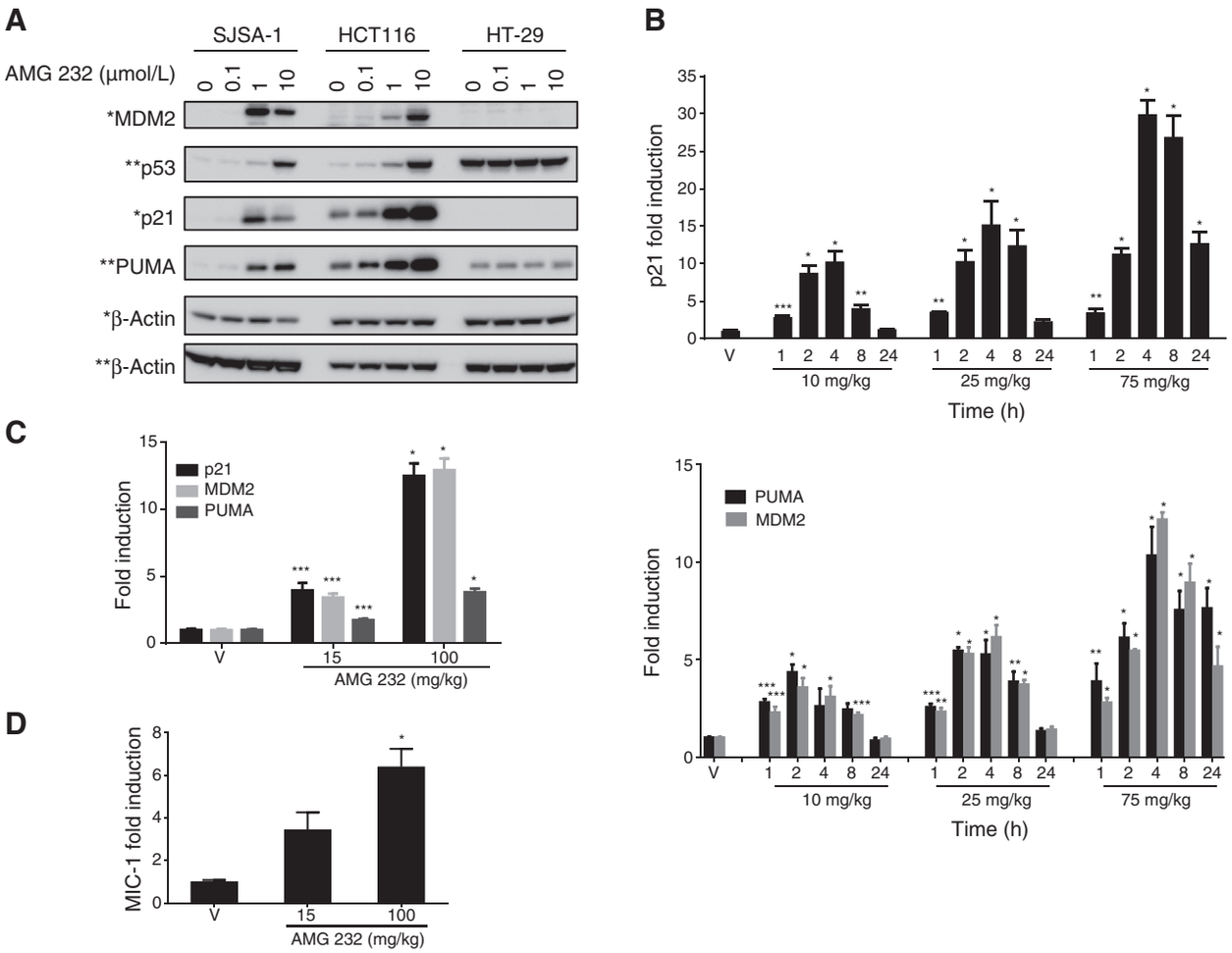

Figure 2.
AMG 232 treatment induces p53 pathway activity *in vitro* and *in vivo*. A, AMG 232 leads to increased p53, p21, MDM2, and PUMA proteins in p53 wild-type cells (SJSA-1, HCT116) but not in p53-mutant HT-29 cells. Because of very high induction of p21 and MDM2 proteins in SJSA-1 cells, reduced protein was loaded (*, 2 μg protein/lane SJSA-1, 20 μg/lane HCT116 and HT-29; **, 20 μg protein/lane all). B, AMG 232 induces p21 (top), MDM2, and PUMA mRNA (bottom) in SJSA-1 tumor cells *in vivo* in a time- and dose-dependent manner. Mice were treated with one dose of AMG 232, and tumors were harvested at the indicated time points and analyzed for transcript levels. C and D, AMG 232 induces p21, MDM2, PUMA, and MIC-1 in HCT116 tumor cells *in vivo*. Mice were treated with AMG 232 once daily for 2 days, and tumors (C) or serum (D) were harvested for analysis 6 hours after the last dose. Data, mean fold increase over vehicle-treated controls ± SEM. $n = 4$/group. *, $P < 0.0001$; **, $P < 0.001$; ***, $P < 0.05$.

models demonstrated a range of *in vivo* antitumor activity of AMG 232. In the HCT116 colorectal cancer model (*KRAS* mutant), the highest dose of AMG 232 resulted in 86% TGI compared with control, and the ED_{50} was 31 mg/kg (Fig. 3C). AMG 232 treatment in an A375sq2 *BRAF*-mutant melanoma model resulted in 97% TGI, with an ED_{50} of 18 mg/kg (Fig. 3E). The NCI-H460 non–small cell lung cancer model was the least sensitive, where AMG 232 treatment resulted in 60% TGI at the highest dose, with an ED_{50} of 78 mg/kg (Fig. 3G). There was no body weight loss in any of the AMG 232 xenograft studies (Supplementary Fig. S3). To note, AMG 232 displays approximately 40-fold less biochemical potency on murine MDM2 compared with human MDM2 (data not shown).

Tumors were harvested at the end of each xenograft study to determine the effect of AMG 232 treatment on p53 pathway activity. AMG 232 treatment resulted in a dose- and time-dependent induction of p21 mRNA compared with vehicle-treated tumors (Fig. 3B, D, F, and H). The level of p21 induction within each tumor model related to the degree of TGI, where p21 levels were highest in tumors whose growth was most inhibited. However, the maximum p21 induction level varied across tumor models.

AMG 232 blocks DNA synthesis and induces apoptosis *in vivo*

To further understand the mechanism whereby AMG 232 caused inhibition of tumor growth *in vivo*, we assessed the effect of AMG 232 treatment on cell cycle and apoptosis. Incorporation of BrdUrd and cleavage of caspase-3 were examined by IHC in the SJSA-1 and HCT116 xenografts, representing, respectively, a model that regresses and a model that undergoes cytostasis after AMG 232 treatment (Fig. 3A and C). Tumor-

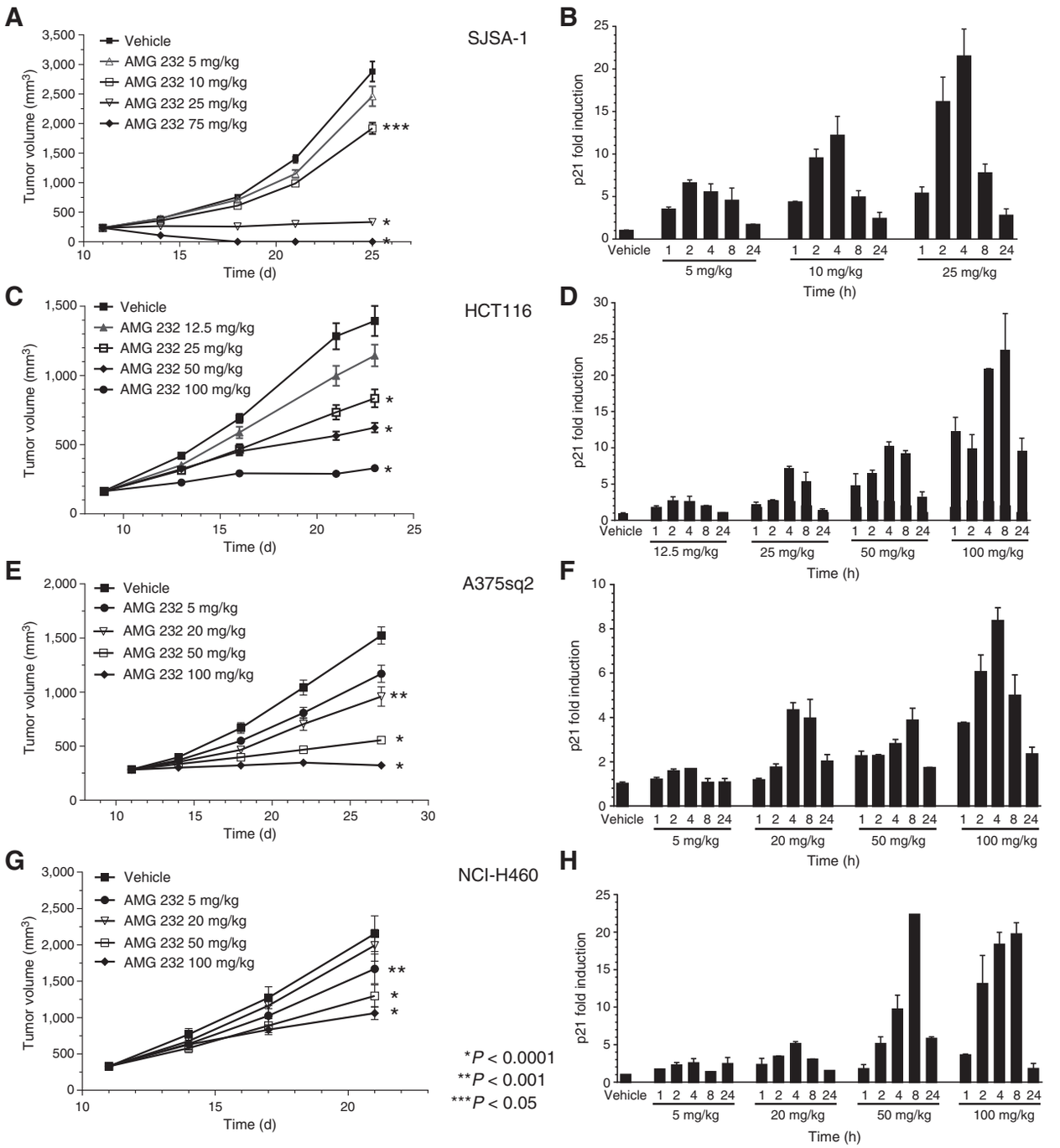

Figure 3.
AMG 232 treatment inhibits tumor growth *in vivo* in a broad range of tumor models. For each xenograft model, the left panel shows the effect of AMG 232 treatment on tumor growth over time ($n = 10$/group), and the right panel is the effect on p21 mRNA induction in tumors taken at the end of the study (at 1, 2, 4, 8, or 24 hours. $n = 2$/time point). Treatment began when tumors reached approximately 200 mm^3, and all groups were treated daily by oral gavage. Data, mean ± SEM. *, $P < 0.0001$; **, $P < 0.001$; ***, $P < 0.05$ compared with vehicle control group. A and B, SJSA-1. C and D, HCT116. E and F, A375sq2. G and H, NCI-H460.

bearing mice were treated daily with AMG 232 or vehicle control, and tumors were harvested 6 hours after one dose (day 1) or four doses (day 4). In the SJSA-1 tumors, there was a significant decrease in BrdUrd incorporation after one dose, and a marked decrease (88%) after 4 days of dosing (Fig. 4A and B), demonstrating a robust inhibition of the cell cycle by AMG 232. Concomitantly, increased cleaved caspase-3 staining was observed after one dose, which was further increased by day 4 when a marked 12-fold induction of cleaved caspase-3 was observed (Fig. 4C and D). In HCT116 tumors, there was no

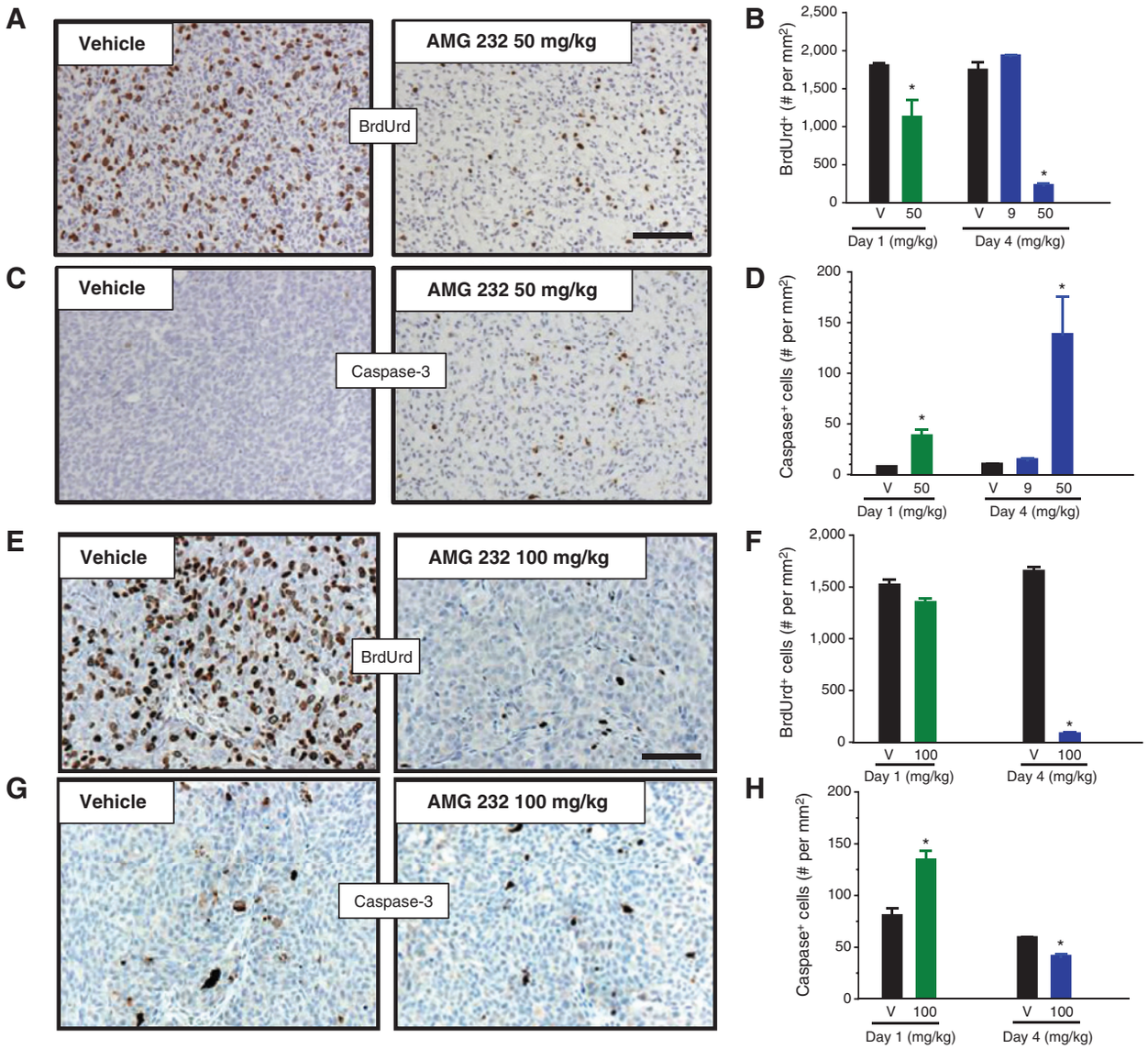

Figure 4.
AMG 232 treatment causes cell-cycle arrest and induces apoptosis *in vivo*. Mice bearing SJSA-1 (A–D) or HCT116 (E–H) tumors were treated with vehicle control or AMG 232 for 4 days. Tumors were harvested 6 hours after treatment on days 1 and 4, fixed, and processed for IHC detection of BrdUrd (A and E) and cleaved caspase-3 (C and G). Representative images of each group are shown from day 4. Bars, 100 μm. B, D, F and H, quantification of the BrdUrd and cleaved caspase-3 staining from each group ($n = 10$/group). Data, mean ± SEM. *, $P < 0.005$.

detectable effect on the cell cycle after one dose (6 hours); however, by day 4, AMG 232 treatment caused a 96% decrease in BrdUrd incorporation (Fig. 4E and F). There was a moderate increase in cleaved caspase-3 staining in HCT116 tumors after one dose, but this effect reversed and after 4 days of AMG 232 treatment cleaved caspase-3 levels were slightly less than control tumors (Fig. 4G and H). Taken together, AMG 232 treatment resulted in marked reductions in BrdUrd incorporation in both tumor models, reflecting a robust arrest of the cell cycle. Apoptosis was induced more dramatically in the SJSA-1 tumor model compared with HCT116, consistent with the observations of tumor regression and cytostasis, respectively, after AMG 232 treatment (Fig. 3A and B).

AMG 232 potentiates the antitumor activity of p53-inducing cytotoxics *in vivo*

We investigated combination treatment of AMG 232 with several standards of care where there was clear biologic rationale to support an interaction in the p53 pathway. Cytotoxic agents that induce DNA damage and p53 activation were evaluated in relevant tumor models. We first tested the combination of AMG 232 with platinum-containing agents in the non–small cell lung cancer model NCI-H460, which is moderately resistant to AMG 232 treatment alone (Fig. 3G). AMG 232 was dosed at its maximally effective dose (100 mg/kg) in this model and was combined with the MTD of cisplatin (5 mg/kg) in mice. Although both agents inhibited tumor

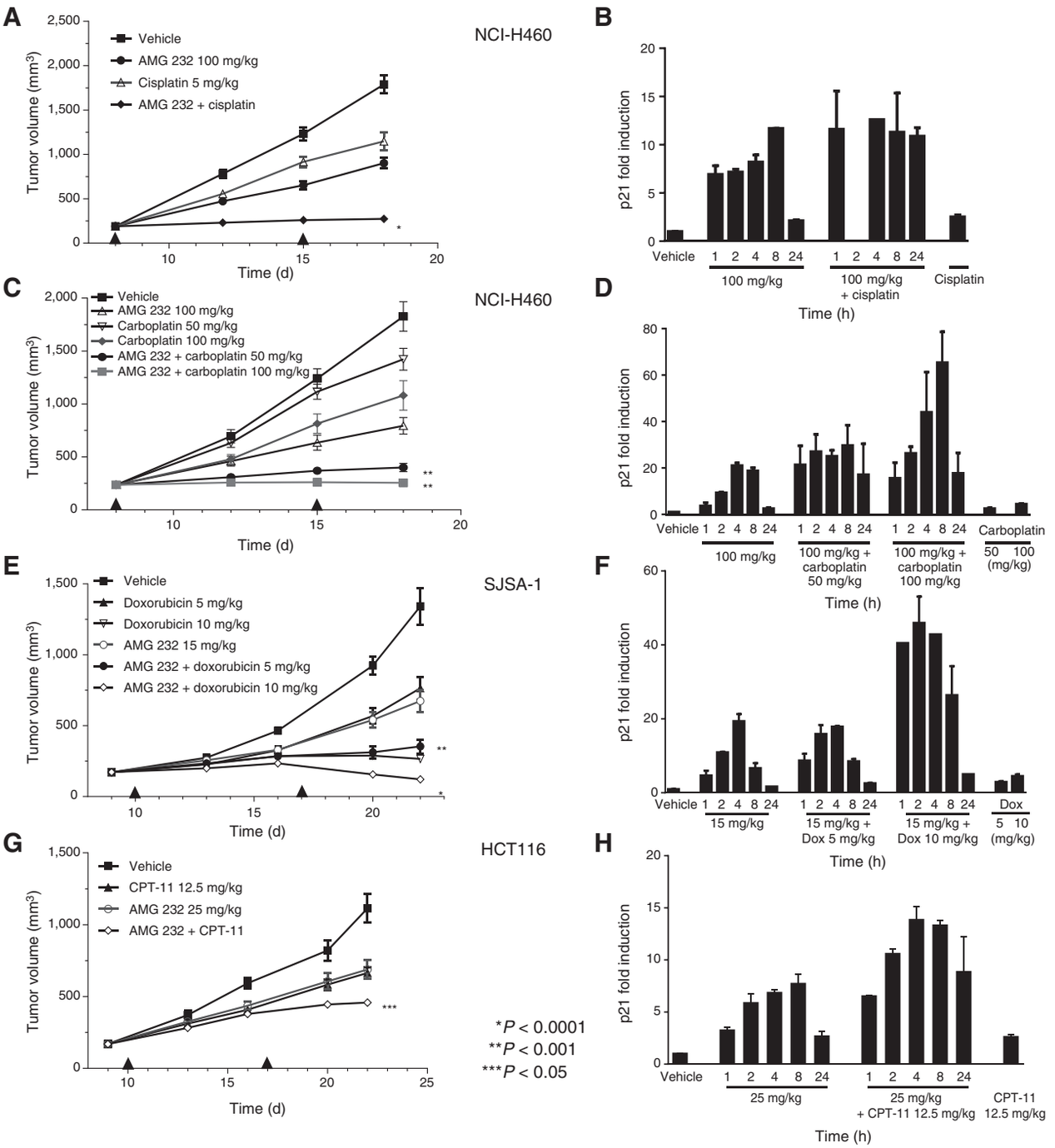

Figure 5.
AMG 232 enhances the antitumor activity of DNA-damaging cytotoxics. AMG 232 or vehicle control was dosed orally once daily in combination with cisplatin (A), carboplatin (C), doxorubicin (E), or CPT-11 (G), which were dosed once weekly (indicated by arrowheads on *x*-axes). Data, mean tumor volume ± SEM ($n = 10$/group). *, $P < 0.0001$; **, $P < 0.005$; ***, $P < 0.05$. *P* values are for comparisons of the combination treatment to each single agent in that combination. B, D, F, H, quantification of p21 mRNA induction in tumors harvested at the end of the xenograft studies. $n = 2$/time point at 1, 2, 4, 8, and 24 hours after last treatment of AMG 232. In B, there was insufficient RNA recovered at the 2-hour time point from the combination group. For p21 analysis in the cytotoxic treatments alone, tumor harvest was 4 days (cisplatin, carboplatin) or 6 days (doxorubicin, CPT-11) after last dose of chemo.

growth compared with vehicle control, the combination treatment resulted in synergistic antitumor efficacy and caused tumor stasis (Fig. 5A). Similarly, we combined AMG 232 (100 mg/kg) with carboplatin at two different doses (50 and 100 mg/kg). In each case, the combination of AMG 232 with carboplatin resulted in superior antitumor efficacy (Fig. 5C).

Notably, the combination with the lower dose of carboplatin (50 mg/kg) resulted in similar antitumor efficacy compared with the combination with the higher dose of carboplatin (100 mg/kg), consistent with a synergistic effect. To determine the effect of combination treatment on p53 pathway activity, tumors were harvested at the end of the studies for p21 analysis. In the AMG 232-cisplatin study, AMG 232 alone induced p21 over time, and p21 levels returned to baseline by 24 hours (Fig. 5B). Cisplatin alone induced p21 minimally (2.5-fold). However, in the AMG 232–cisplatin combination, p21 levels were elevated more than 10-fold, which was sustained across the full 24 hours. Similarly, in the AMG 232–carboplatin combination study, the amplitude and duration of p21 induction in the combination treatments were markedly higher than either of the single-agent treatments (Fig. 5D), with a peak of >60-fold induction of p21 in the higher dose combination group. Of note, the last cisplatin and carboplatin doses were administered 4 days before the end of the study and tumor harvest, indicating a prolonged and sustained combination effect on p53 pathway activation.

We tested the combination of AMG 232 with doxorubicin in the SJSA-1 sarcoma model. The SJSA-1 model is sensitive to AMG 232 treatment alone (Fig. 3A), therefore a suboptimal dose (15 mg/kg) of AMG 232 was used for this combination. As single agents, both dose levels of doxorubicin and AMG 232 alone inhibited tumor growth compared with the control group (Fig. 5E). In combination, AMG 232 plus doxorubicin resulted in superior antitumor efficacy, with the higher dose combination (doxorubicin 10 mg/kg) resulting in tumor regression. Induction of p21 by doxorubicin treatment alone (10 mg/kg) was approximately 5-fold. AMG 232 treatment alone resulted in peak p21 induction of approximately 20-fold. However, p21 levels were elevated approximately 40-fold in the higher dose combination treatment group (Fig. 5F), indicating that p53 pathway activation was highest in tumors that regressed. Furthermore, the increased p21 induction in this combination group was prolonged 6 days after the final dose of doxorubicin.

We also evaluated the combination of AMG 232 with irinotecan (aka, CPT-11) in the HCT116 colorectal carcinoma model. The combination treatment resulted in significantly improved antitumor efficacy compared with the single agents (Fig. 5G). Similarly, p21 levels were induced higher and for a longer duration after combination treatment (Fig. 5H) compared with the single-agent treatments. There was no significant body weight loss in any of the combination studies (Supplementary Fig. S3).

Discussion

Herein, we have characterized the *in vitro* and *in vivo* attributes of AMG 232, the most potent MDM2 inhibitor described to date. AMG 232 binds to MDM2 with picomolar affinity (K_D 0.045 nmol/L) and inhibits the MDM2–p53 interaction in a biochemical cell-free assay with an IC_{50} of 0.6 nmol/L. Treatment of tumor cells with AMG 232 *in vitro* resulted in robust activation of the p53 pathway leading to inhibition of proliferation. Tumor cells underwent growth arrest, and this was related to induction of p21, a direct transcriptional target of p53 and a mediator of cell-cycle arrest. AMG 232 treatment also resulted in stabilization of p53 protein and increased levels of MDM2, p21, and PUMA proteins in p53 wild-type cells. In a broad panel of tumor cell lines, AMG 232 treatment inhibited the growth of p53 wild-type cells in a 3-day viability assay, whereas there was no significant effect on p53-mutant tumor cells (Fig. 1A). This suggests that the antiproliferative response to AMG 232 is dependent on p53. However, we did not investigate the possible role of other p53 family members (e.g., p73) in this study. The maximum antitumor effect of AMG 232 treatment varied across the p53 wild-type cells with some cell lines undergoing complete cell killing whereas others were cytostatic (Fig. 1B). This observation is consistent with other reports, suggesting that the propensity of tumor cells to undergo apoptosis after MDM2 inhibition varies across cell lines (9).

Pharmacodynamic assays revealed that AMG 232 caused potent activation of p53 signaling *in vivo*. The exceptional *in vivo* properties of AMG 232 led to significant induction of p21, MDM2, and PUMA expression for 24 hours after a single dose (Fig. 2B). Induction of p21 occurred in SJSA-1 cells, which undergo complete cell killing *in vitro*, as well as in HCT116 cells that reflect a growth-arrest phenotype. This suggests that cell-cycle arrest via p21 activity occurs as an initial response to MDM2 inhibition independent of the ultimate outcome of inhibition of proliferation and/or apoptosis. PUMA induction was more pronounced in SJSA-1 tumors compared with HCT116 tumors, consistent with their apoptotic versus growth-arrest phenotypes, respectively.

AMG 232 demonstrated antitumor activity *in vivo* in a variety of tumor types with different genetic backgrounds. The MDM2-amplified SJSA-1 model was the most sensitive to AMG 232 treatment, which caused complete tumor regression and no evidence of tumor regrowth after cessation of treatment. AMG 232 was also effective at inhibiting tumor growth in models that harbor mutations in MAPK signaling pathways (e.g., *KRAS*-mutant HCT116 and *BRAF*-mutant A375), indicating that restoration of p53 tumor-suppressive function is broadly effective in tumors that are p53 wild-type. Tumor regression was not observed in all models, indicating that some tumor cells are more resistant to undergoing apoptosis after MDM2 inhibition. *In vivo* mechanism of action studies assessing cell-cycle progression (BrdUrd) and cell death (cleaved caspase-3) demonstrated that AMG 232 induced rapid cell-cycle arrest in both SJSA-1 and HCT116 tumors, but marked induction of apoptosis was observed only in the SJSA-1 line.

Given the high genetic diversity of tumors and frequent emergence of resistance to targeted and cytoxic agents in the clinic, MDM2 inhibitors will likely be combined with other therapies to achieve better clinical responses. To that end, we evaluated combination treatment with several cytotoxic agents where there was mechanistic rationale for an antitumor interaction with MDM2 inhibition. Cisplatin and carboplatin are platinum-based chemotherapeutics that bind and cross-link DNA, causing inhibition of DNA repair and synthesis (16). They are standards of care for various cancers, including lung and ovarian carcinomas. Doxorubicin is an anthracycline that intercalates DNA and blocks the progression of topoisomerase-2, inhibiting DNA replication (17). It is used to treat a wide range of cancers, including hematologic malignancies and sarcomas. Irinotecan (aka CPT-11) is a topoisomerase-1 inhibitor and leads to DNA fragmentation and inhibition of replication, and is primarily used to treat colorectal carcinomas (17). The mechanism of tumor cell death by DNA-damaging cytotoxic drugs like these is largely mediated by induction of

the p53 pathway (18), which leads to growth arrest and apoptosis. However, the full tumor-killing potential of such agents may be limited by insufficient p53 activity in tumor cells that may have faulty cell-cycle checkpoint controls. We hypothesized that combining MDM2 inhibition with such agents may restore the full tumor-suppressive function of p53 and increase antitumor efficacy. We tested this hypothesis by combining AMG 232 with these agents in relevant tumor models. In each case, the addition of MDM2 inhibition by AMG 232 to chemotherapy treatment led to significantly improved antitumor efficacy, and this was related to a marked increase in p53 signaling as evidenced by dramatic and sustained induction of p21 in the combination treatment groups lasting 4 to 6 days after the last doses of chemotherapies.

The data presented here support the investigation of AMG 232 treatment alone, and in combination with standard-of-care agents, in patients with cancer. AMG 232 is currently being evaluated in clinical trials.

Disclosure of Potential Conflicts of Interest

J.D. Oliner has immediate family members with ownership interest (including patents) in Amgen. A. Coxon has ownership interest in Amgen Inc. stock. No potential conflicts of interest were disclosed by the other authors.

Authors' Contributions

Conception and design: J. Canon, S.H. Olson, Q. Ye, L. Jin, S. Kaufman, R. Kendall, J.D. Oliner, A. Coxon, R. Radinsky

Development of methodology: J. Canon, T. Osgood, A.Y. Saiki, R. Robertson, D. Yu, J. Zhou, S. Kaufman

Acquisition of data (provided animals, acquired and managed patients, provided facilities, etc.): J. Canon, T. Osgood, S.H. Olson, A.Y. Saiki, R. Robertson, D. Yu, A. Chen, D. Cordover, S. Kaufman

Analysis and interpretation of data (e.g., statistical analysis, biostatistics, computational analysis): J. Canon, T. Osgood, A.Y. Saiki, R. Robertson, D. Yu, J. Eksterowicz, Q. Ye, J. Zhou, D. Cordover, S. Kaufman, J.D. Oliner, A. Coxon, R. Radinsky

Writing, review, and/or revision of the manuscript: J. Canon, T. Osgood, S.H. Olson, Q. Ye, S. Kaufman, R. Kendall, J.D. Oliner, A. Coxon, R. Radinsky

Administrative, technical, or material support (i.e., reporting or organizing data, constructing databases): T. Osgood, R. Robertson, Q. Ye, S. Kaufman

Study supervision: J. Canon, T. Osgood, R. Radinsky

Acknowledgments

The authors thank Annie Luo, Darlene Kratavil, Chris De La Torre, Gwyneth Van, and Efrain Pacheco for IHC and histology support.

The costs of publication of this article were defrayed in part by the payment of page charges. This article must therefore be hereby marked *advertisement* in accordance with 18 U.S.C. Section 1734 solely to indicate this fact.

Received August 25, 2014; revised December 18, 2014; accepted December 22, 2014; published OnlineFirst January 7, 2015.

References

1. Vogelstein B, Lane D, Levine AJ. Surfing the p53 network. Nature 2000; 408:307–10.
2. Vazquez A, Bond EE, Levine AJ, Bond GL. The genetics of the p53 pathway, apoptosis and cancer therapy. Nat Rev Drug Discov 2008;7:979–87.
3. Olivier M, Hollstein M, Hainaut P. TP53 mutations in human cancers: origins, consequences, and clinical use. Cold Spring Harb Perspect Biol 2010;2:a001008.
4. Chene P. Inhibiting the p53-MDM2 interaction: an important target for cancer therapy. Nat Rev Cancer 2003;3:102–9.
5. Harris SL, Levine AJ. The p53 pathway: positive and negative feedback loops. Oncogene 2005;24:2899–908.
6. Oliner JD, Pietenpol JA, Thiagalingam S, Gyuris J, Kinzler KW, Vogelstein B. Oncoprotein MDM2 conceals the activation domain of tumour suppressor p53. Nature 1993;362:857–60.
7. Vassilev LT, Vu BT, Graves B, Carvajal D, Podlaski F, Filipovic Z, et al. *In vivo* activation of the p53 pathway by small-molecule antagonists of MDM2. Science 2004;303:844–8.
8. Mohammad RM, Wu J, Azmi AS, Aboukameel A, Sosin A, Wu S, et al. An MDM2 antagonist (MI-319) restores p53 functions and increases the life span of orally treated follicular lymphoma bearing animals. Mol Cancer 2009;8:115.
9. Tovar C, Graves B, Packman K, Filipovic Z, Higgins B, Xia M, et al. MDM2 small-molecule antagonist RG7112 activates p53 signaling and regresses human tumors in preclinical cancer models. Cancer Res 2013;73:2587–97.
10. Rew Y, Sun D, Gonzalez-Lopez De Turiso F, Bartberger MD, Beck HP, Canon J, et al. Structure-based design of novel inhibitors of the MDM2-p53 interaction. J Med Chem 2012;55:4936–54.
11. Ding Q, Zhang Z, Liu JJ, Jiang N, Zhang J, Ross TM, et al. Discovery of RG7388, a potent and selective p53-MDM2 inhibitor in clinical development. J Med Chem 2013;56:5979–83.
12. Sun D, Li Z, Rew Y, Gribble M, Bartberger MD, Beck HP, et al. Discovery of AMG 232, a potent, selective, and orally bioavailable MDM2-p53 inhibitor in clinical development. J Med Chem 2014;57: 1454–72.
13. Carnahan J, Beltran PJ, Babij C, Le Q, Rose MJ, Vonderfecht S, et al. Selective and potent Raf inhibitors paradoxically stimulate normal cell proliferation and tumor growth. Mol Cancer Ther 2010;9:2399–410.
14. Carry JC, Garcia-Echeverria C. Inhibitors of the p53/hdm2 protein-protein interaction-path to the clinic. Bioorg Med Chem Lett 2013;23: 2480–5.
15. Masuya K, Furet P, Stutz S, Holzer P, Pissot-Soldmann C, Buschmann N, et al.Discovery of CGM097 as a novel Mdm2 inhibitor[abstract]. In: Proceedings of the 105th Annual Meeting of the American Association for Cancer Research; 2014 Dec 5–9; San Diego, CA. Abstract nr DDT01-01.
16. Poklar N, Pilch DS, Lippard SJ, Redding EA, Dunham SU, Breslauer KJ. Influence of cisplatin intrastrand crosslinking on the conformation, thermal stability, and energetics of a 20-mer DNA duplex. Proc Natl Acad Sci U S A 1996;93:7606–11.
17. Pommier Y, Leo E, Zhang H, Marchand C. DNA topoisomerases and their poisoning by anticancer and antibacterial drugs. Chem Biol 2012; 17:421–33.
18. Lakin ND, Jackson SP. Regulation of p53 in response to DNA damage. Oncogene 1999;18:7644–55.